Fabrication of morphology-controlled TiO_2 photocatalyst nanoparticles and improvement of photocatalytic activities by modification of Fe compounds

Teruhisa Ohno, Yin Yang

Department of Materials Science, Graduate School of Engineering, Kyushu Institute of Technology, Fukuoka 804-8550, Japan

tohno@che.kyutech.ac.jp

Abstract

Our previous studies suggested that redox reaction proceeded separately on specific exposed crystal faces of TiO_2 nanoparticles. Site-selective deposition of metal or metal oxide on TiO_2 specific exposed crystal faces successfully proceeded using the unique reactivity properties on the surface of TiO_2 nanoparticles under photoexcitation.

A remarkable improvement of photocatalytic activity of shape-controlled brookite and rutile TiO_2 nanorods with modification of Fe^{3+} compounds was observed under visible light. Crystal face-selective metal compound modification on exposed crystal faces of TiO_2 nanorods with brookite and rutile phases were successfully prepared. Brookite and rutile TiO_2 nanorods prepared by site-selective modification with metal compounds should be ideal visible-light responsive TiO_2 photocatalysts because of the remarkable suppression of back electron transfer from TiO_2 to oxidized metal compounds on the surface of the TiO_2 nanorod with a brookite or rutile phase.

In this manuscript, the development of exposed crysta face-controlled TiO_2 nanorods with rutile and brookite phases was described. The obtained rutile and brookite TiO_2 nanorod, showing remarkably high activity for degradation of organic compounds compared to the photocatalytic activities of anatase fine particles (ST-01), is one of the most active commercially available photocatalysts for environmental cleanup in Japan. The technology of visible light-responsive treatment for morphology-controlled rutile and brookite TiO_2 nanorods by crystal face-selective modification of Fe^{3+} compounds was also discussed in this paper. The Fe^{3+} compound-modified rutile and brookite TiO_2 nanorods show much higher activity than that of conventional visible light-responsive N-doped TiO_2, which is commercially available in Japan.

Keywords Morphology-controlled TiO_2; Separation of reaction sites; Visible-light responsive TiO_2 loaded with Fe^{3+}

1. Introduction

TiO_2 has been intensively investigated over the past several decades for its environmental cleanup and solar light energy conversion applications because of its stable physical-chemical properties, low cost and high activity [1-9]. TiO_2 has three kinds of crystal faces: rutile, anatase and brookite. The particle shapes, nano-scale morphologies, and crystallinity of rutile were clarified and can be controlled [9-11]. The surface chemistry of single crystalline rutile particles is also studied intensively because their chemical activity depends greatly on surface structures and exposed crystal faces [12].

Well-crystallized faceted TiO_2 nanoparticles showed a drastic improvement of photocatalytic activity compared to that of normal spherical TiO_2 fine particles with poor crystallinity [13]. Therefore, attention has been paid to the preparation of TiO_2 nanoparticles with control of exposed crystal faces for improvement of their photocatalytic activity. Among the various methods for synthesis of TiO_2 nanoparticles, hydrothermal treatment is thought to be one of the best candidates for TiO_2 synthesis because TiO_2 nanoparticles with good morphology control using additives for exposing crystal faces are obtained under mild conditions. Recently, morphology-controlled TiO_2 nanoparticles with anatase, rutile, and brookite phases have been prepared by these techniques. [14-19]

The development of visible light-responsive TiO_2 photocatalysts using impurity doping has proceeded over the past few decades [20-25]. However, impurity doping sometimes increase defects in the lattice of TiO_2, resulting in a decrease in photocatalytic activity because the defects work as recombination centers [26, 27]. Recently, unique visible-light responsive TiO_2 photocatalysts loaded with metal ions such as Fe^{3+} and Cu^{2+} have been reported [28-32]. This is an interesting method for fabrication of visible light-responsive TiO_2 without defects. However, back electron transfer between injected electrons from a metal sensitizer in the TiO_2 bulk and oxidized metal ions loaded on the surface of TiO_2 may easily proceed and result in a significant decrease in photocatalytic activity under visible light. Therefore, it is necessary for new discovery for development metal compounds modified TiO_2 showing visible light responsibility.

2. Exposed crystal face-controlled rutile TiO_2 nanorod

The procedure for synthesis of an exposed crystal face-controlled rutile TiO_2 nanorod is as follows. A chemical solution was put in a sealed Teflon-lined autoclave reactor containing an aqueous solution of titanium trichloride ($TiCl_3$) and sodium chloride (NaCl). The solution was then put into a 200 ^oC oven for 48 h. The precipitate was collected and dried in a vacuum oven. Samples are

referred to as SH1 (NaCl 1 mol·L^{-1}), SH3 (NaCl 3 mol·L^{-1}), and SH5 (NaCl 5 mol·L^{-1}). SH5 is the optimized preparation condition for the highest photocatalytic activity.

Reduction and oxidation sites on the exposed crystal faces of a rutile TiO_2 nanorod were assigned by the photodeposition technique for Pt and PbO_2, respectively. A rutile TiO_2 nanorod aqueous suspension containing 2-propanol and hexachloroplatinic acid ($H_2PtCl_6 \cdot 6H_2O$) was irradiated with a mercury ultraviolet-visible (UV) lamp (light intensity: 1.0 mW·cm^{-2}). N_2 gas was purged through the suspension in order to remove oxygen prior to UV irradiation. After irradiation, the color of the powder changed from white to gray-silver, and the suspension was collected (Pt-loaded rutile TiO_2 nanorod) and dried at 70 °C under reduced pressure for 24 h. In order to determine the oxidation site on the surface of a rutile TiO_2 nanorod, photodeposition of PbO_2 was performed by using the same light source as that in the case of photodeposition of Pt. Pt-loaded rutile TiO_2 nanorod suspension containing $Pb(NO_3)_2$ was irradiated under an aerated condition [14-19, 33]. After the reaction, the color of the powder changed from gray-silver to brown, indicating that PbO_2 was deposited on the surface of the rutile TiO_2 nanorod. Pt and PbO_2 particles deposited on a rutile TiO_2 nanorod were analyzed by scanning electron microscope (SEM), energy dispersive X-ray spectrometry (EDX) and transmission electron microscope (TEM).

The photocatalytic activity of TiO_2 nanoparticles was evaluated by photodecomposition of acetaldehyde. Changes in the concentration of acetaldehyde and evolved CO_2 as a function of irradiation time were analyzed. TiO_2 powder was spread on the bottom of a glass dish, and the glass dish was placed in a Tedlar bag. 500×10^{-6} acetaldehyde was prepared in the vessel. Irradiation was conducted at room temperature after equilibrium between the gas and adsorbed acetaldehyde was reached. A 500 W Xe-lamp with a UV-35 filter to cut off wavelengths shorter than 350 nm was used as a light source. After starting the irradiation, the decreases in acetaldehyde concentration and evolved CO_2 concentration were determined by using a gas chromatograph. ST-01 having anatase phase fine TiO_2 produced by Ishihara Sangyo CO. Ltd. and MT-600 having rutile phase produced by Teyca Co. Ltd. were usually used as reference catalysts.

XRD patterns of all of the obtained particles were assigned to pure rutile phase and no other phases were detected (Fig.1). The mean grain size was determined from Scherrer's equation. The average crystallite sizes (relative surface areas) of the samples were found to be 66.0 nm (32.8 $m^2 \cdot g^{-1}$), 72.7 nm (26.0 $m^2 \cdot g^{-1}$) and 97.2 nm (12.1 $m^2 \cdot g^{-1}$) for SH1, SH3 and SH5, respectively. Figure 2 shows TEM image and selected area electron diffraction (SAED) patterns. The particle morphology was rod shape as shown in TEM image. The SAED patterns of the exposed surface of the end of the rod and side surface of the rod were assigned to (111) and (110), respectively.

Figure 3 shows the photocatalytic evolution of CO_2 by decomposition of acetaldehyde on reference TiO_2 and SH5 under UV light irradiation at a light intensity of 10 $mW \cdot cm^{-2}$. Photocatalytic activities of rutile TiO_2 nanorods were much higher than those of MT-600 and ST-01. The order of photocatalytic activities was SH5 > ST-01 > MT-600B as shown in Fig.3. Separation of reaction sites on the surface of a rutile TiO_2 nanorod might be important for improvement of its photocatalytic activity. Moreover, it is expected that the efficiency of electron-hole separation would be enhanced because of the difference in the number of trap sites for electrons such as Ti ions and for holes such as oxygen on the exposed crystal surfaces.

Figure 4 shows SEM image of rutile TiO_2 nanorods loaded with Pt for the reduction site ((110) face) and loaded with PbO_2 for the oxidation site ((111) face). Spatial separation of reaction sites on exposed crystal face-controlled rutile TiO_2 nanorods is thought to be effective for improvement of photocatalytic reactions because of the suppression of back reaction on the surface of the TiO_2 photocatalyst.

Different surface energy levels of the conduction and valence bands are expected for different crystal faces of TiO_2 because of the characteristic of atomic arrangements of these faces. For instance, trapped holes are mainly accumulated at an oxygen-rich crystal face, which might be assigned to anoxidation site. On the other hand, crystal face rich in Ti^{4+} atoms results in the accumulation of electrons to generate Ti^{3+}, which might be assigned to a reduction site. These properties lead to the separation of electrons and holes [14]. The effective separation of oxidation and reduction sites of rutile TiO_2 nanorods suggests that the electronic energy levels of the (110) face are lower than those of the (111) face as shown in Fig.4 [34]. The large specific surface areas and small crystal sizes as well as high crystallinity of TiO_2 might play important roles in the enhancement of photocatalytic activities. In addition, spatial separation of reaction sites on the photocatalyst nanoparticle by controlling the exposed crystal surface of a rutile TiO_2 nanorod is a more important factor for improvement of photocatalytic activity because a rutile TiO_2 nanorod with a small surface area (10-30 $m^2 \cdot g^{-1}$) showed a higher photocatalytic activity than that of ST-01 with a large surface area (300 $m^2 \cdot g^{-1}$).

3. Visible light-responsive rutile TiO_2 nanorod modified with Fe^{3+} compounds

The procedure for non-site-selective modification of Fe^{3+} compounds on the entire surface of rutile TiO_2 nanorods is as follows. An aqueous suspension of morphology-controlled rutile TiO_2 nanorods with an aqueous solution of $Fe(NO_3)_3$ was stirred under an aerated condition. After filtration, the residue was washed with deionized water and dried under reduced pressure.

The procedure for preparation of visible-light responsive rutile TiO_2 nanorods site-selective modified with Fe^{3+} compounds is as follows. An aqueous suspension consisting of rutile TiO_2 nanorods and an aqueous solution of $Fe(NO_3)_3$ with ethanol was stirred under an aerated condition by bubbling N_2 gas. Photo-reduction of Fe^{3+} loaded on reduction crystal faces ({110} faces) of rutile TiO_2 nanorods proceeded during UV irradiation. Fe^{2+} compounds on the reduction sites of rutile TiO_2 nanorods, which were generated by reduction of Fe^{3+}, were dissolved in aqueous phase. The residue was separated by filtration immediately after the photoirradiation. The residue was washed with deionized water and dried under reduced pressure (Fig.5).

Photocatalytic activities of the samples were evaluated by photocatalytic decomposition of acetaldehyde. A glass dish containing a sample was placed in a 125 ml Tedlar bag. 500×10^{-6} gaseous acetaldehyde was injected into the Tedlar bag, and photoirradiation was performed at room temperature. The gaseous composition in the Tedlar bag was 79% N_2, 21% O_2, < 0.1×10^{-6} CO_2 and 500×10^{-6} acetaldehyde, and relative humidity was 30% (ca.). An light-emitting diode (LED) emitting light at a wavelength of ca. 455 nm (±15 nm) with an intensity of 1.0 $mW\cdot cm^{-2}$ was used for visible light irradiation. The concentrations of CH_3CHO and CO_2 were estimated by gas chromatography.

Double-beam photoacoustic spectroscopy was used to elucidate the electron transfer between rutile TiO_2 nanorods and Fe^{3+} compounds loaded on the oxidation sites of rutile TiO_2 nanorods. A TiO_2 sample was placed in a photoacoustic (PA) cell. The atmosphere was controlled by a flow of nitrogen containing ethanol vapor (N_2+EtOH) or artificial air containing ethanol vapor (air+EtOH). An LED emitting light at ca. 625 nm was used as a probe light, and the output intensity was modulated by a digital function generator. A blue LED (emitting light at ca. 470 nm, 8.1 $mW\cdot cm^{-2}$) was also used as simultaneous continuous irradiation for photoexcitation. The PA signal acquired by a condenser microphone buried in the cell was amplified and monitored by a digital lock-in amplifier. Detailed setups of double-beam photoacoustic (DB-PA) spectroscopic measurements were reported previously [35].

The rutile TiO_2 nanorods were prepared according to our previous studies [15, 16]. Rutile TiO_2 nanorods used in this study have {110} and {111} exposed crystal faces. The specific surface area of the bare rutile rod was 12.1 $m^2\cdot g^{-1}$.

The valence state of iron compounds on rutile TiO_2 nanorods was confirmed by XPS analysis to be trivalent state. It was reported that Fe^{2+} was hardly adsorbed on the TiO_2 surface compared to Fe^{3+} compounds [36]. Therefore, Fe^{2+} produced by reduction of Fe^{3+} by photoexcited electrons on reduction sites of rutile TiO_2 nanorods from the TiO_2 surface diffused into aqueous media. Our previous study suggested that reduction and oxidation on a rutile TiO_2 nanorod proceeded

predominantly on {110} and {111} exposed crystal faces [28]. Therefore, Fe^{3+} are expected to be mainly adsorbed on {111} faces under UV irradiation because Fe^{3+} on {110} faces are desorbed due to reduction of Fe^{3+} to Fe^{2+} (Fig.5). Modification of Fe^{3+} induced a color change from white to pale yellow as reported previously [32]. Figure 6 show UV-Vis spectra of bare and site-selective Fe^{3+}-modified rutile TiO_2 nanorods and non-site-selective Fe^{3+}-modified rutile TiO_2 nanorods. In the wavelength region between 400 and 500 nm of DR spectra, a red shift of the photoabsorption edge was observed.

Photocatalytic activity for decomposition of acetaldehyde over Fe^{3+}-modified rutile TiO_2 nanorod was evaluated under visible light irradiation. Figure 7 shows the amount of evolved CO_2 as a result of acetaldehyde degradation under visible-light irradiation for 24 h. Photocatalytic activity of Fe^{3+}-modified rutile TiO_2 nanorod was higher than that of visible light-responsive N-doped TiO_2 (N-TiO_2; Sumitomo Chemical Co.). This result indicates that Fe^{3+} compound modification of a rutile TiO_2 nanorod induces a photocatalytic reaction under visible-light irradiation as follows [32]. The photoexcited Fe^{3+} compound loaded on a rutile TiO_2 nanorod injected electrons into the conduction band of the rutile TiO_2 nanorod, resulting in an oxidized state of Fe^{3+} (Fe^{4+}). The injected electrons migrated to the surface of the rutile TiO_2 nanorod and reduced oxygen species. The oxidized state of the Fe^{3+} compound (Fe^{4+}) oxidized organic compounds such as acetaldehyde and returned to the initial state of the metal ion compound (Fe^{3+}). A site-selective modified Fe^{3+} rutile TiO_2 nanorod showed higher photocatalytic activity than that of N-doped TiO_2. Moreover, the photocatalytic activity of Fe^{3+}-modified rutile TiO_2 showed a dependence on its preparation method (site-selective modified Fe^{3+} rutile TiO_2 nanorod > non-site-selective modified Fe^{3+} rutile TiO_2 nanorod). A plausible reason for the difference in photocatalytic activity is site selectivity of Fe^{3+} modification. The following experiments were carried out to determine the reason.

The same modification method was applied to commercial rutile TiO_2 without specific exposed crystal faces. Therefore, UV irradiation during Fe^{3+} modification is thought to induce non-site-selective modification on the particles because a redox reaction proceeds in the neighboring sites without being separated. The amounts of evolved CO_2 evolution as a result of decomposition of acetaldehyde over site-selective and non-site-selective Fe^{3+}-modified commercial rutile TiO_2 were 495×10^{-6} and 500×10^{-6}, respectively under visible light irradiation for 24 h. These two samples were prepared by different modification methods, but the same net amounts of Fe^{3+} compound were loaded on these rutile samples by adjusting the initial amount of Fe^{3+}. The photocatalytic activities of these samples were similar with or without UV irradiation during Fe^{3+} modification. This indicates that the UV irradiation induced formation of the same Fe^{3+} species for

photocatalytic reaction as that in the case of non-site-selective modification of Fe^{3+} on a rutile TiO_2 nanorod. Therefore, the reason for the high activity of site-selective Fe^{3+} modified samples is that UV irradiation during Fe^{3+} modification induces loading of site-selective Fe^{3+} compounds on rutile TiO_2 nanorod.

Properties of electron injection in the conduction band of TiO_2 were observed by DB-PAS [35]. Figure 8 shows PA intensities for a non-site-selective Fe^{3+}-modified rutile TiO_2 nanorod and a site-selective Fe^{3+}-modified rutile TiO_2 nanorod as a function of irradiation time of visible-light in the presence of N_2+EtOH. PA intensity increased with visible light irradiation because Ti^{4+} was reduced to Ti^{3+} by injected electrons from the photoexcited Fe^{3+} compound loaded on the rutile TiO_2 nanorod. The saturation limit of PA intensity showed no dependence on Fe^{3+} modification conditions. This is a reasonable result because the amounts of photoabsorption of these samples were not so different as shown in Fig. 6. This indicates that the plausible factor may be efficiency of reduction on rutile TiO_2 nanorods modified with Fe^{3+} by injected electrons.

DB-PA measurements in the presence of oxygen with EtOH were also carried out to elucidate the behavior of injected electrons in the rutile TiO_2 nanorod. Figure 9 shows time-course curves of a non-site-selective Fe^{3+}-modified rutile TiO_2 nanorod and a site-selective Fe^{3+}-modified rutile TiO_2 nanorod under visible-light irradiation in the presence of air+EtOH. The steady-state value of PA intensity showed a dependence on the modification method (non-site-selective Fe^{3+}-modified rutile TiO_2 nanorod > site-selective Fe^{3+}-modified rutile TiO_2 nanorod). This suggests that the efficiency of reduction on the surface of a site-selective Fe^{3+}-modified rutile TiO_2 nanorod is higher than that on a non-site-selective Fe^{3+}-modified rutile TiO_2 nanorod because the consumption of injected electrons in the rutile TiO_2 nanorod by reduction of oxygen efficiently proceeded on the {110} face without retardation.

4. Morphology-controlled brookite TiO_2 nanorod with exposed crystal faces

Morphology-controlled brookite TiO_2 nanorods with {210} and {212} exposed crystal faces were prepared by hydrothermal synthesis [19, 37-42]. The procedure for preparation of morphology-controlled brookite TiO_2 with exposed crystal faces is as follows. Amorphous titanium hydroxide particles were dispersed in 30% hydrogen peroxide containing ammonia and glycolic acid. After stirring the solution at ca. 60 °C for several hours, an orange gelled compound was obtained. The gelled compound was dispersed in deionized water with pH being adjusted to 10 by the addition of ammonia. The solution in a Teflon bottle sealed with a stainless jacket was heated at 200 ^{o}C for 48 h in an oven. After hydrothermal treatment, the residue was washed with deionized water and dried under reduced pressure at 60 ^{o}C for 12 h.

For controlling the aspect ratio (AR) of brookite of a TiO_2 nanorod, the preparation procedure was modified as follows. Amorphous titanium hydroxide particles were dispersed in 30% hydrogen peroxide containing ammonia and glycolic acid, and a yellow peroxo titanic acid (PTA) solution was obtained. An aqueous solution containing an appropriate amount of PVA (5, 25, or 50 mg) was added to the PTA solution and the solution was stirred at room temperature for 6 h. After the treatment, an orange gelled compound was obtained. The gelled compound was dispersed in deionized water with pH being adjusted to 10. The solution in a Teflon bottle sealed with a stainless jacket was heated at 200 ^oC for 48 h in an oven. After hydrothermal treatment, the residue in the Teflon bottle was washed with milli-Q water until ionic conductivity of the supernatant was < 10 $S \cdot cm^{-1}$. The particles were dried under reduced pressure at 60 ^oC for 12 h.

Figure 11 shows XRD patterns of prepared TiO_2 nanorod particles, which are assigned to a pure brookite phase. Surface areas of the brookite TiO_2 nanorods prepared with 5, 25 and 50 mg of PVA were 24.2, 25.8, and 27.7 $m^2 \cdot g$, respectively. Figure 12 shows TEM image of brookite TiO_2 without a polymer. A brookite TiO_2 nanorod with a length of 100 nm, width of 25 nm and AR of 2.7 was obtained. The relative surface area of the prepared brookite TiO_2 nanorod was 47 $m^2 \cdot g^{-1}$. Exposed crystal faces were analyzed by TEM and SAED analysis and were assigned to large {212} and small {210} exposed crystal faces (Fig. 11). The {210} and {212} exposed crystal faces on the brookite TiO_2 nanorod were assigned to reduction and oxidation sites using previously reported technique [15-17]. Therefore, Fe^{3+} are expected to mainly adsorb on {212} faces under UV irradiation because Fe^{3+} on {210} faces desorb due to reduction of Fe^{3+} to Fe^{2+} (Fig.5). Fe^{2+} were recovered to Fe^{3+} as a result of reoxidation by oxygen and/or positive holes on {212} faces.

TEM images of AR-controlled brookite TiO_2 by addition of the PVA polymer are shown in Fig.12. The results indicate that addition of 50 mg PVA was sufficient to prepare brookite TiO_2 particles with the smallest AR (Fig. 12). TEM images of samples prepared with and without PVA are shown in Fig. 13.

Photocatalytic activities for photocatalytic decomposition of toluene over a brookite TiO_2 nanorod were evaluated. 100 mg powder was spread on a glass dish, which was placed in a Tedlar bag. Five hundred parts per million of gaseous acetaldehyde or one hundred parts per million of gaseous toluene was injected into the Tedlar bag. The gaseous composition in the Tedlar bag was 79% N_2, 21% O_2, < 0.1×10^{-6} CO_2 and 100×10^{-6} or 500×10^{-6} toluene, and relative humidity was ca. 30%. A light-emitting diode with a center wavelength of ca. 365 nm (0.1 $mW \cdot cm^{-2}$) was used as the light source. The concentrations of acetaldehyde and carbon dioxide (CO_2) were analyzed by gas chromatography.

The photocatalytic activities of the prepared samples for decomposition of toluene were evaluated. Figure 14 shows CO_2 evolution as a result of toluene decomposition over several kinds of brookite TiO_2 under UV LED irradiation for 8 h. The AR of a brookite TiO_2 nanorod with specific exposed crystal faces was rather sensitive to photocatalytic activity for toluene decomposition. Toluene decomposition on a photoirradiated brookite TiO_2 nanorod with a larger AR showed higher photocatalytic activity than that on a brookite TiO_2 nanorod with a smaller AR. This result suggested that photocatalytic activity for toluene decomposition increased with an increase in the AR of the brookite TiO_2 nanorod. Under optimized conditions, reduction sites on the surface of the brookite TiO_2 nanorod should be predominantly exposed as shown in Fig. 14. These results indicated that reduction of oxygen on the surfaces of the reduction sites of a brookite TiO_2 nanorod might be the rate-determining step for toluene oxidation over a brookite TiO_2 nanorod under UV light.

5. Visible light-responsive brookite TiO_2 nanorod modified with Fe^{3+} compounds

For non-site-selective Fe^{3+} compound modification of a brookite TiO_2 nanorod, an aqueous suspension containing shape-controlled brookite TiO_2 nanorods and an aqueous solution of iron(III) nitrate ($Fe(NO_3)_3$) was stirred for 6 h under an aerated condition. The supernatant and residue were separated by filtration, and the residue was washed with deionized water and dried under reduced pressure.

For site-selective Fe^{3+} compound modification of a brookite TiO_2 nanorod, an aqueous suspension containing each brookite TiO_2 and an aqueous solution of $Fe(NO_3)_3$ with ethanol was stirred for 6 h under an aerated condition. The stirring was carried out under UV irradiation with a 500-W super-high-pressure mercury lamp (1.0 $mW \cdot cm^{-2}$). The supernatant and residue were separated by filtration immediately after stirring for 6 h. The residue was washed with deionized water and dried under reduced pressure.

The color of the brookite TiO_2 nanorod changed from white to pale yellow. Figure 15 shows UV-Vis spectra of bare and Fe^{3+}-modified brookite TiO_2. An increase in photoabsorption was observed in the wavelength region between 400 and 500 nm of DR spectra. Photoabsorption increased with an increase in the net amount of Fe^{3+} compounds loaded on the brookite TiO_2 nanorod.

Photocatalytic activities for decomposition of acetaldehyde over the samples were analyzed. 100 mg powder was spread on a glass dish, which was placed in a 125 cm^3 Tedlar bag. Five hundred parts per million of gaseous acetaldehyde was injected into the Tedlar bag. The gaseous composition in the Tedlar bag was 79% N_2, 21% O_2, < 0.1×10^{-6} CO_2 and 500×10^{-6} acetaldehyde,

and relative humidity was ca. 30%. A light-emitting diode (LED, Lumileds, Luxeon LXHL-NRR8) that emitted light at a wavelength of 455 nm (1.0 $mW \cdot cm^{-2}$) was used. The concentrations of acetaldehyde and carbon dioxide (CO_2) were estimated by gas chromatography.

Figure 16 shows the dependence of the site-selective Fe^{3+} compound-modified brookite TiO_2 on photocatalytic activity (CO_2 evolution as a result of acetaldehyde degradation after 24 h of photoirradiation). Photocatalytic activity of the Fe^{3+}-modified brookite TiO_2 nanorod was much higher than that of the Fe^{3+}-modified commercial spherical brookite TiO_2. Under visible light irradiation, no photocatalytic activity of the bare brookite TiO_2 nanorod ore bare commercial brookite TiO_2 nanoparticles for oxidation of acetaldehyde was observed. This indicates that Fe^{3+} on the brookite TiO_2 nanorod induced photocatalytic reaction under visible-light irradiation [26]. The amount of evolved CO_2 over nitrogen-doped TiO_2 (N-TiO_2; Sumitomo Chemical Co.) was about 180×10^{-6} under the same experimental conditions. The Fe^{3+}-modified brookite TiO_2 nanorod showed much higher photocatalytic activity than that of N-TiO_2.

Photocatalytic activity increased with an increase in the amount of Fe^{3+} modification because of the increase in visible light photoabsorption. In addition, an excess amount of Fe^{3+} modification decreased photocatalytic activity presumably due to a decrease in reduction sites by coverage of the TiO_2 surface. Therefore, an increase in photocatalytic activity of the site-selective Fe^{3+}-modified brookite TiO_2 nanorod might be attributable to the removal of an excess amount of Fe^{3+} compounds. In addition, a site-selective Fe^{3+} modified brookite TiO_2 nanorod with a larger AR showed higher photocatalytic activity for acetaldehyde degradation than that of a brookite TiO_2 nanorod site-selectively modified with Fe^{3+} compounds having a smaller AR. These results suggested that the rate-determining step of acetaldehyde oxidation under visible light might be oxygen reduction proceeding on the reduction site of the brookite TiO_2 nanorod. Therefore, a site-selective Fe^{3+} modified brookite TiO_2 nanorod with a larger AR having a large reduction area showed the highest activity for acetaldehyde oxidation under visible light.

The same modification method was applied to commercial brookite TiO_2 that has a spherical shape without specific exposed crystal faces. Figure 16 shows the amount of CO_2 evolution over site-selective Fe^{3+}-modified commercial brookite TiO_2 nanoparticles under visible-light irradiation. The photocatalytic activity of Fe^{3+}-modified commercial brookite TiO_2 is quite low compared to that of the site-selective Fe^{3+}-modified brookite TiO_2 nanorod because UV irradiation during Fe^{3+} modification does not induce site-selective modification on the commercial brookite TiO_2 nanoparticles due to the redox reaction proceeding in the neighboring sites without being separated.

6. Conclusion

It is demonstrated that the morphology of rutile and brookite TiO_2 particles can be controlled by means of a hydrothermal process with morphology-controlled reagents. The addition of PVP and PVA to the hydrothermal preparation process for a brookite TiO_2 nanorod reduces the AR of the brookite TiO_2 nanorod (AR ~ 1.6-5.2). The exposed crystal surfaces of rutile and brookite TiO_2 nanorods show different activities: oxidation and reduction. The photocatalytic activities of rutile and brookite TiO_2 nanorods are higher than that of anatase or brookite TiO_2 fine particles that are commercially available in Japan. It is found that the photocatalytic activity depends not on the relative surface area but on the surface structure of TiO_2 nanorods, suggesting that prevention of electron-hole pair recombination plays an important role during the photodegradation of organic compounds.

Fe^{3+}-modification on shape-controlled rutile and brookite TiO_2 nanorods results in high photocatalytic activity under visible-light irradiation because Fe^{3+} are site-selectively modified on {111} and {212} exposed crystal faces and redox reactions are spatially separated. DB-PA analyses indicate that photocatalytic activity is determined by not efficiency of electron injection but efficiency of reduction by injected electrons. The efficiency of reduction is influenced by site-selectivity of Fe^{3+}-modification on {111} faces because Fe^{3+} on {110} faces retard an efficient reduction on the bare TiO_2 surface.

Acknowledgements

This work was financially supported by the Advanced Catalytic Transformation Program for Carbon Utilization (ACT-C), Japan Science and Technology Agency (JST).

References

[1] Yu J, Low J, Xiao W, Zhou P, Jaroniec M. Enhanced Photocatalytic CO_2-Reduction Activity of Anatase TiO_2 by Coexposed {001} and {101} Facets. J. Am. Chem. Soc. 2014 :136 :8839.

[2] Huang Z, Sun , Lv K, Zhang Z, Li M, Li B. Effect of contact interface between TiO_2 and g-C_3N_4 on the photoreactivity of g-C_3N_4/TiO_2 photocatalyst: (0 0 1) vs (1 0 1) facets of TiO_2. Appl. Catal. B : Environnemental. 2015 :164 :420.

[3] Zhou P, Wu J, Yu W, Zhao G, Fang G, Cao S. Vectorial doping-promoting charge transfer in anatase TiO_2 {0 0 1} surface. Appl. Sur. Sci. 2014 :319 :167.

[4] Wang C, Hu Q, Huang J, Zhu C, Deng Z, Shi H, Wu L, Liu Z, Cao Y. Enhanced hydrogen production by water splitting using Cu-doped TiO_2 film with preferred (0 0 1) orientation. Appl. Sur. Sci. 2014 :292 :161.

[5] Ren C, Wang G, Chen Y, Chen Y. Degradation of benzene on Zr-doped TiO_2 photocatalysts with a bimodal pore size distribution. Rare Metals. 2014 :33 :714.

[6] Lv K, Cheng B, Yu J, and Liu G. Fluorine ions-mediated morphology control of anatase TiO_2 with enhanced photocatalytic activity. Phys. Chem. Chem. Phys. 2012 :14 :5349.

[7] Hoffmann M R, Martin S T, Choi W, Bahnemann D W. Environmental applications of semiconductor photocatalysis. Chem Rev. 1995 : 95:69.

[8] Choi W. Pure and modified TiO_2 photocatalysts and their environmental applications. Catal Surv Asia. 2006 : 10 :16.

[9] Chen X, Mao S S. Titanium dioxide nanomaterials: Synthesis, properties, modifications, and applications. Chem Rev. 2007 : 107:2891

[10] Hosono E, Fujihara S, Kakiuchi K, Imai H. Growth of submicrometer-scale rectangular parallelepiped rutile TiO_2 films in aqueous $TiCl_3$ solutions under hydrothermal conditions. J Am Chem Soc. 2004 : 126:7790.

[11] Neale N R, Frank A J. Size and shape control of nanocrystallites in mesoporous TiO_2 films. J Mater Chem. 2007 17:3216.

[12] Huang X, Pan C. Large-scale synthesis of single-crystalline rutile TiO_2 nanorods via a one-step solution route. J Cryst Growth. 2007 : 306:117.

[13] Testino A, Bellobono I R, Buscaglia V, Canevali C, D`Arienzo M, Polizzi S, Scotti R, Morazzoni F. Optimizing the photocatalytic properties of hydrothermal TiO_2 by the control of phase composition and particle morphology. A systematic approach. J Am Chem Soc. 2007 : 129:3564.

[14] Ohno T, Sarukawa K, Matsumura M. Crystal faces of rutile and anatase TiO_2 particles and their roles in photocatalytic reactions. New J Chem. 2002 : 26:1167.

[15] Bae E, Murakami N, Ohno T. Exposed crystal surface-controlled TiO_2 nanorods having rutile phase from $TiCl_3$ under hydrothermal conditions. J Mol Catal A: Chem. 2009 : 300:72.

[16] Bae E, Ohno T. Exposed crystal surface-controlled rutile TiO_2 nanorods prepared by hydrothermal treatment in the presence of poly(vinyl pyrrolidone). Appl Catal B: Environ. 2009 : 91: 634.

[17] Bae E, Murakami N, Nakamura M, Ohno T. Effect of chemical etching by sulfuric acid or H_2O_2–NH_3 mixed solution on the photocatalytic activity of rutile TiO_2 nanorods. Appl Catal A: Gen. 2010 : 380:48

[18] Murakami N, Kurihara Y, Tsubota T, Ohno T. Shape-controlled anatase titanium(IV) oxide particles prepared by hydrothermal treatment of peroxo titanic acid in the presence of polyvinyl alcohol. J Phys Chem C. 2009 : 113:3062.

[19] Ohno T, Higo T, Saito H, Yuan S, Jin Z, Yang Y, Tsubota T. Dependence of photocatalytic activity on aspect ratio of a brookite TiO_2 nanorod and drastic improvement in visible light responsibility of a brookite TiO_2 nanorod by site-selective modification of Fe^{3+} on exposed faces. J Mol Catal A: Chem. 2015 : 396:261.

[20] Sato, S. Photocatalytic activity of nox-doped TiO_2 in the visible-light region. Chem Phys Lett. 1986 ; 123:126.

[21] Asahi R, Morikawa, T, Ohwaki T, Aoki K, Taga Y. Visible-light photocatalysis in nitrogen-doped titanium oxides. Science. 2001 : 293:269.

[22] Umebayashi T, Yamaki T, Itoh H, Asai K. Band gap narrowing of titanium dioxide by sulfur doping. Appl Phys Lett. 2002 : 81:454.

[23] Ohno T, Akiyoshi M, Umebayashi T, Asai K, Mitsui T, Matsumura M. Preparation of S-doped TiO_2 photocatalysts and their photocatalytic activities under visible light. Appl Catal A: Gen. 2004 : 265:115.

[24] Ohno T, Tsubota T, Nishijima K, Miyamoto Z. Degradation of methylene blue on carbonate species-doped TiO_2 photocatalysts under visible light. Chem Lett. 2004 : 33:750.

[25] Irie H, Watanabe Y, Hashimoto K. Carbon-doped anatase TiO_2 powders as a visible-light sensitive photocatalyst. Chem Lett. 2003 : 32:772.

[26] Serpone N, Lawless D. Spectroscopic, photoconductivity, and photocatalytic studies of tio2 colloids - naked and with the lattice doped with Cr^{3+}, Fe^{3+}, and V^{5+} cations. Langmuir. 1994 : 10:643.

[27] Ikeda S, Sugiyama N, Pal B, Marci G, Palmisano L, Noguchi H, Uosakid K, Ohtani B. Photocatalytic activity of transition-metal-loaded titanium(IV) oxide powders suspended in aqueous solutions: Correlation with electron-hole recombination kinetics. Phys Chem Chem Phys. 2001 : 3:267.

[28] Kisch H, Zang L, Lange C, Maier W F, Antonius C, Meissner D. Modified, amorphous titania - a hybrid semiconductor for detoxification and current generation by visible light. Angew Chem Int Ed. 1998 : 37: 3034.

[29] Zang L, Lange C, Abraham I, Storck S, Maier W F, Kisch H. J. Phys. Chem. B. 1998 : 102 :10765.

[30] Zang L, Lange C, Abraham I, Storck S, Maier W F, Kisch H. Amorphous microporous titania modified with platinum(IV) chloride - A new type of hybrid photocatalyst for visible light detoxification. J Phys Chem B. 1998 : 102:10765.

[31] Macyk W, Kisch H. Photosensitization of crystalline and amorphous titanium dioxide by platinum(IV) chloride surface complexes. Chem Eur J. 2001 : 7:1862.

[32] Murakami N, Chiyoya T, Tsubota T, Ohno T. Switching redox site of photocatalytic reaction on titanium(IV) oxide particles modified with transition-metal ion controlled by irradiation wavelength. Appl Catal A: Gen. 2008 : 348:148.

[33] Murakami N, Ono A, Nakamura M, Tsubota T, Ohno T. Development of a visible-light-responsive rutile rod by site-selective modification of iron(III) ion on {111} exposed crystal faces. Appl Catal A: Gen. 2010 : 97:115.

[34] Oliver P M, Watson G W, Kelsey E T, Parker. S C. Atomistic simulation of the surface structure of the TiO_2 polymorphs rutile and anatase. J Mater Chem. 1997 : 7:563.

[35] Murakami N, Mahaney O O P, Abe R, Torimoto T, Ohtani B. Double-beam photoacoustic spectroscopic studies on transient absorption of titanium(IV) oxide photocatalyst powders. J Phys Chem C. 2007 : 111:11927.

[36] Ohno T, Haga D, Fujihara K, Kaizaki K, Matsumura M. Unique effects of iron(III) ions on photocatalytic and photoelectrochemical properties of titanium dioxide. J Phys Chem B. 1997 : 101:6415.

[37] Kandiel T A, Feldhoff A, Robben L, Dillert R, Bahnemann D W. Tailored titanium dioxide nanomaterials: anatase nanoparticles and brookite nanorods as highly active photocatalysts. Chem Mater. 2010 : 22:2050.

[38] Kobayashi M, Tomita K, Petrykin V, Yin S, Sato T, Yoshimura M, Kakihana M. Hydrothermal synthesis of nanosized titania photocatalysts using novel water-soluble titanium complexes. Solid State Phenomena. 2007 : 124-126 :723.

[39] Zhang H, Banfield J F. Understanding polymorphic phase transformation behavior during growth of nanocrystalline aggregates: insights from TiO_2. J Phys Chem B. 2000 : 104 :3481.

[40] Kobayashi M, Petrykin V, Kakihana M, Tomita K. Hydrothermal synthesis and photocatalytic activity of whisker-like rutile-type titanium dioxide. J Am Ceram Soc. 2009: 92(S1): S21.

[41] Murakami N, Kamai T, Tsubota T, Ohno T. Novel hydrothermal preparation of pure brookite-type titanium(IV) oxide nanocrystal under strong acidic condition. Catal. Commun. 2009 :10 :963.

[42] Ma Z, Zhang Q, Liu J, Yan C, Zhang M, Ohno T. Preparation of luminescent polystyrene microspheres via surface-modified route with rare earth (Eu^{3+} and Tb^{3+}) complexes linked to 2, 2'-bipyridine. Rare Metals. 2013: 30: 1.

Figs

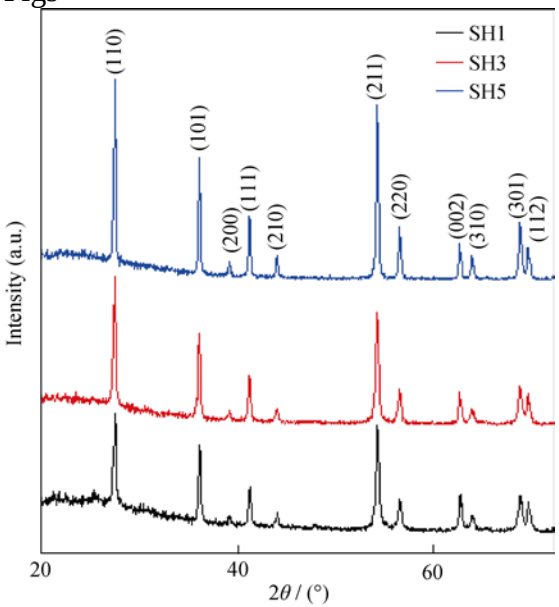

Fig. 1 XRD patterns of SH1, SH3, and SH5.

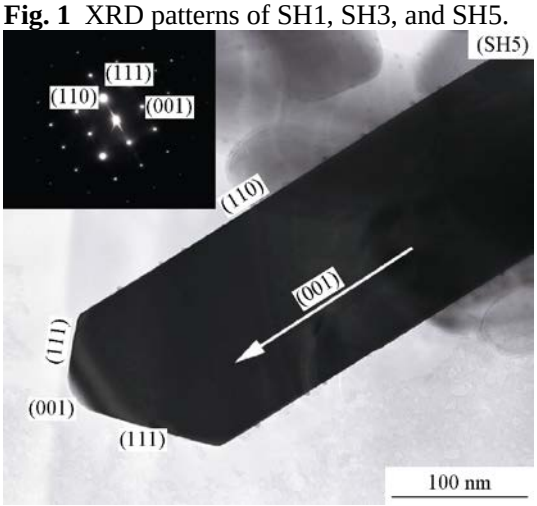

Fig. 2 TEM image and SAED pattern (insert) of SH5.

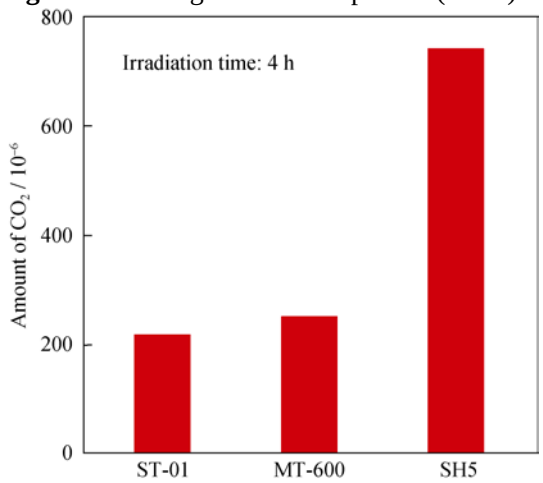

Fig. 3 Amount of evolved CO_2 as a result of decomposition of acetaldehyde on rutile TiO_2 nanorod. Light intensity:10 $mW \cdot cm^{-2}$, irradiation time: 4h, acetaldehyde: 500×10^{-6}

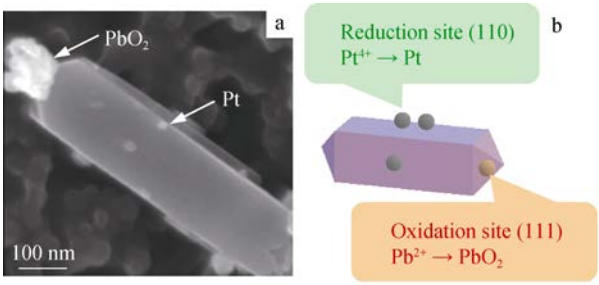

Fig. 4 SEM image of rutile TiO_2 nanorod on which Pt and PbO_2 particles being deposited for reduction site and oxidation site, respectively **a**; schematic representation of Pt or PbO_2 deposition mechanism and assignment of reaction sites **b**.

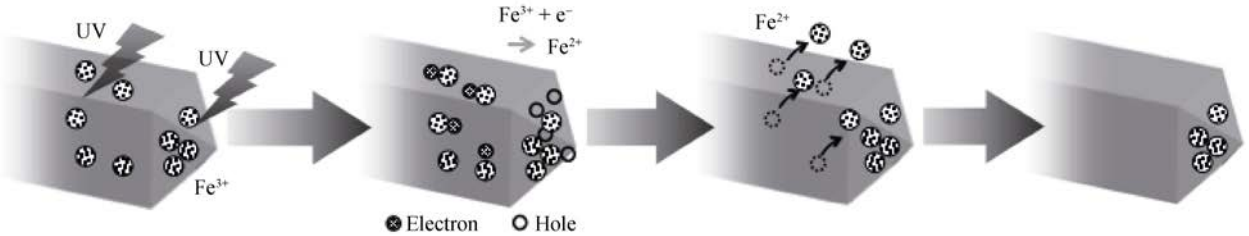

Fig.5 Site selective modification on shape controlled rutile rod with {110} and {111} exposed crystal faces

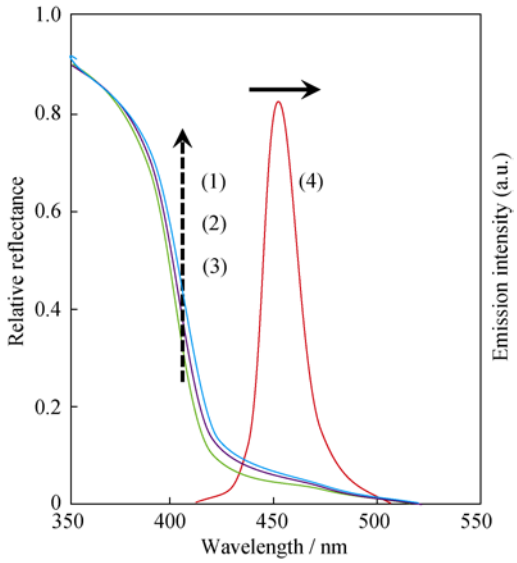

Fig. 6 UV-Vis spectra of (1) non-site-selective Fe^{3+} modified rutile TiO_2 nanorod, (2) site-selective Fe^{3+} modified rutile TiO_2 nanorod, (3) rutile TiO_2 nanorod without modification of Fe^{3+} compounds and (4) emission spectrum of LED used for photocatalytic evaluation

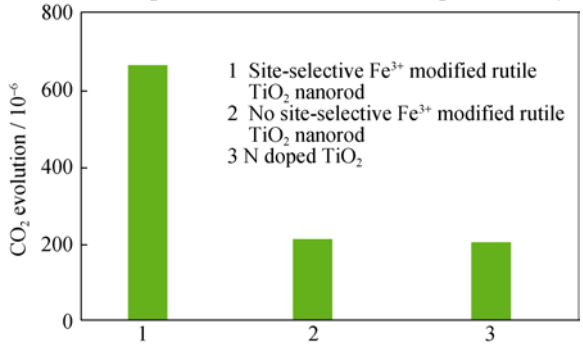

Fig. 7 Amount of evolved CO_2 as a result of acetaldehyde decomposition over Fe^{3+} modified rutile TiO_2 nanorod and N-doped TiO_2 under visible-light irradiation

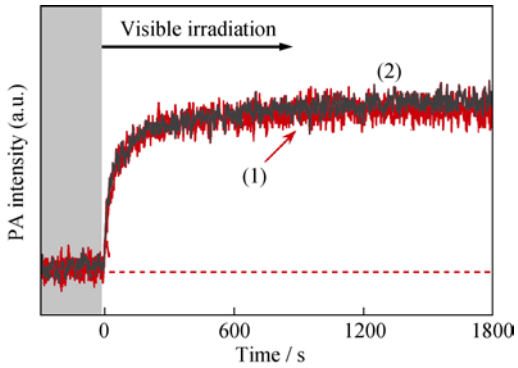

Fig. 8 Time-course curves of PA signals of (1) no site-selective Fe^{3+} modified rutile TiO_2 nanorod and (2) site-selective Fe^{3+} modified rutile TiO_2 nanorod under visible-light irradiation in presence of N_2+EtOH

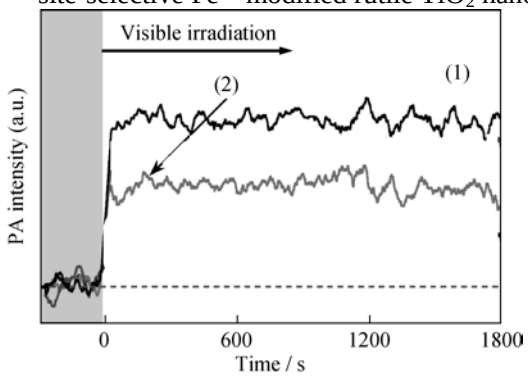

Fig. 9 Time-course curves of PA signals with 50 points smoothing of (1) no site-selective Fe^{3+} modified rutile TiO_2 nanorod and (2) site-selective Fe^{3+} modified rutile TiO_2 nanorod under visible-light irradiation in presence of air + EtOH

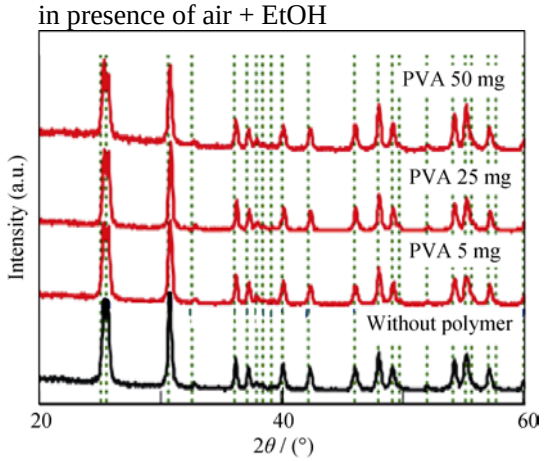

Fig. 10 XRD patterns of prapared TiO_2 nanorods.

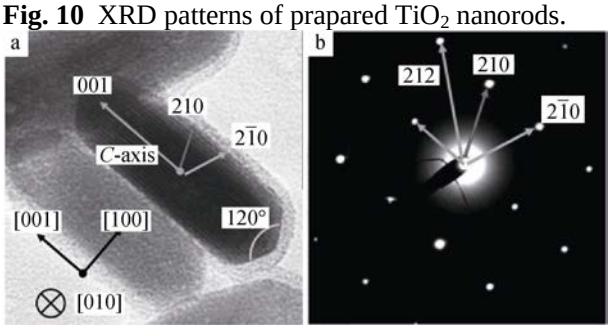

Fig. 11 TEM image of brookite TiO_2 nanorod **a** and SAED analysis of prepared brookite TiO_2 without a polymer **b**

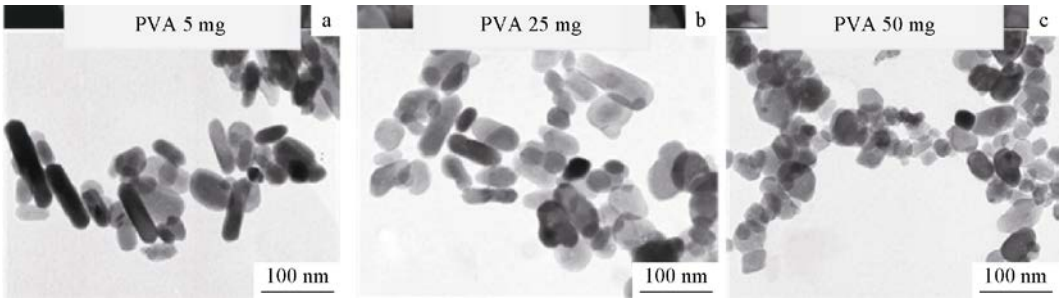

Fig. 12 Influence of addition of PVA on aspect ratio (AR) of brookite TiO_2 nanorods: **a** 5 mg, **b** 25 mg, and **c** 50 mg.

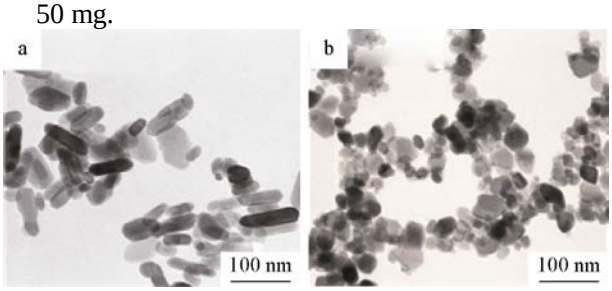

Fig. 13 TEM images of prepared brookite TiO_2 nanorod: **a** AR=2.7, without a polymer; **b** AR=1.6, with PVA (50 mg)

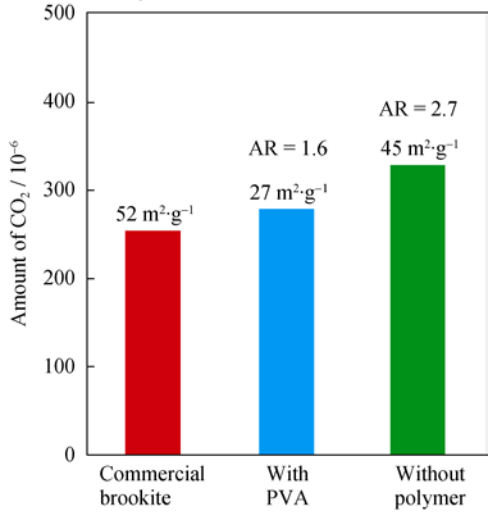

Fig. 14 CO_2 evolution as a result of toluene decomposition over three kinds of prepared brookite TiO_2 under UV LED irradiation for 8 h

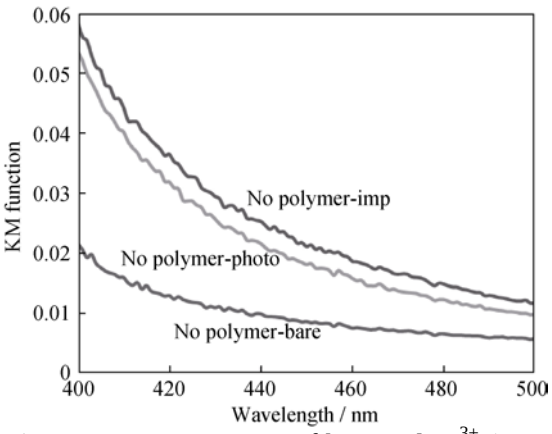

Fig. 15 UV-Vis spectra of bare and Fe^{3+} (0.05 wt%)-modified brookite TiO_2 without a polymer. Imp meaning non-site-selective Fe^{3+} compound modification of brookite TiO_2 and photo meaning site-selective Fe^{3+} compound modification of brookite TiO_2.

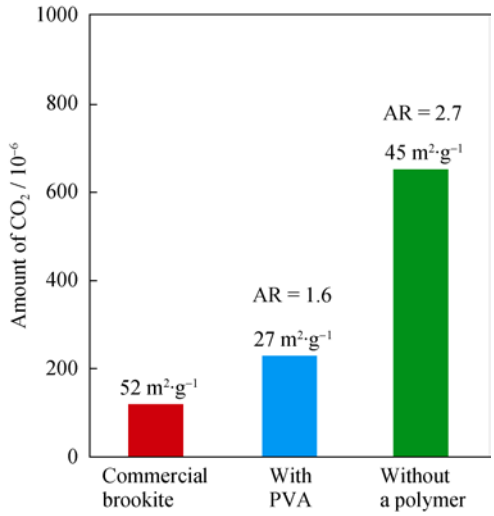

Fig. 16 CO_2 evolution as a result of acetaldehyde decomposition over several kinds of Fe^{3+}(0.05 wt%)-modified brookite TiO_2 under visible light irradiation for 24 h by using an LED at a wavelength of 455 nm